J. Fluid Mech. (1981), *vol.* 105, *pp.* 193–218
Printed in Great Britain

Effects of exit Mach number and temperature on mean-flow and turbulence characteristics in round jets

By J. C. LAU†
Lockheed-Georgia Company, Marietta, Georgia U.S.A.

(Received 21 May 1979 and in revised form 11 July 1980)

This paper describes mean-flow and turbulence measurements conducted in a round jet over a range of Mach numbers from 0·3 to 1·7 and jet-exit static temperatures from − 40 to over 400 °C. It is a continuation of an earlier work, reported by Lau, Morris & Fisher (1979), to try to map the distribution of the various flow characteristics in the jet flow field and to observe the effects of changing jet exit conditions. In the earlier study, the effort was confined to isothermal jets at a limited number of exit Mach numbers, and the laser velocimeter proved to be a particularly useful instrument, especially in situations where the more severe flow conditions made it impossible to extract fluctuating-velocity data by any other means. The present effort capitalizes on this aspect of the velocimeter and also its ability to measure mean velocities accurately; and the extended range and detail of jet conditions chosen for this study is intended to provide a clearer understanding of the effects of systematically changing the jet conditions. Corresponding Pitot and total temperature measurements are also carried out under a representative set of jet conditions specifically to try to shed light on the effect of jet heating. Based on the various axial and radial distributions which are obtained, a picture is constructed of the changing boundaries of the shear layer with changing jet conditions.

1. Introduction

The present study is aimed at observing the changes in the distributions of various flow characteristics in the jet as the exit conditions are changed. It is an extension of an earlier study (Lau *et al.* 1979; hereinafter referred to as I) in which only a cursory view was taken of the effects of exit Mach number in jets which issue at the same *static* temperature as the ambient air (i.e. isothermal jets). In the present effort, the gaps between those earlier test conditions are filled in and the range of exit Mach number and static temperature are extended.

The test programme is summarized in figure 1. The ordinate of the chart gives the ratio of the static jet temperature at the exit plane (T_J) to the ambient temperature (T_0), and the abscissa the ratio of the jet exit velocity (U_J) to the ambient speed of sound (a_0). The oblique curves represent lines of constant Mach number. The grid of selected test points therefore allows the changing jet pattern to be viewed from different perspectives. To a fluid dynamicist who is used to viewing the flow structure in terms of Mach number, the test points forming lines of constant Mach number constitute important points of reference. On the other hand, to the aero-acoustician,

† Now with Kimberly-Clark Corporation, Neenah, Wisconsin, U.S.A.

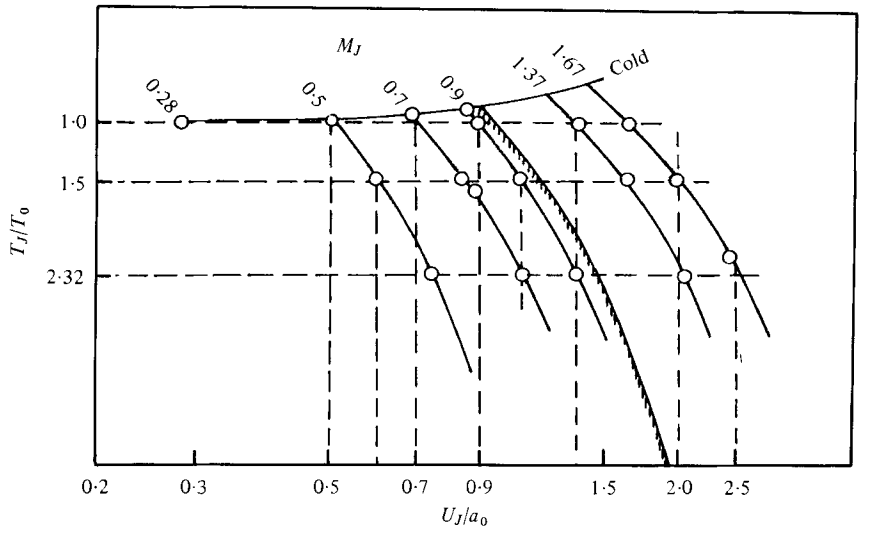

FIGURE 1. Test plan (○, test points).

accustomed to relating the far-field noise intensities to the jet exit velocity, the test points on the constant-velocity lines would provide useful insights.

As in the earlier paper, this one concentrates on data which is generally obtained at individual points in the free-flow field. In particular, the distributions of the mean velocities, turbulence intensities and covariances are compared. Other turbulence characteristics which are obtained by two-point cross-correlation techniques are discussed in another paper (Lau 1980; hereinafter referred to as II).

The velocity at a point in the flow field is a function of the total pressure and temperature at the point. To understand their individual contributions, especially in the cases when the jet is heated, a survey is also made of the distribution of total pressure and temperature in the flow field for a limited number of jet exit conditions.

The capabilities of the laser velocimeter (LV) were assessed earlier (I) by a comparative study of LV and hot-wire measurements in an unheated jet at a low Mach number. It was found that the LV gave mean velocity readings which were comparable to those from the hot-wire. Turbulence intensity data from the LV and the hot-wire also showed the same trends. For example, radial distributions of the turbulence intensity peaked at about the same position and the spectra at corresponding points in the flow exhibited the same appearance. In particular, the peaks which feature so prominently in the spectra of hot-wire signals within the potential core of round jets (Bradshaw, Ferris & Johnson 1964) also appeared in the LV spectra and occurred at the same Strouhal number.

The magnitudes of the turbulence intensity measured with the LV were, however, systematically higher than those measured with a hot-wire, and this was also discovered in an independent study by Barnett & Giel (1976). After an extensive study of the possible sources of error, it now seems fairly clear (Whiffen, Lau & Smith 1979; II) that a substantial portion of the discrepancy may be due to an error in the LV data and methods have been devised which would eliminate the discrepancy in the measurement (Lau *et al.* 1981).

The main body of the results is presented in two sections. The mean-flow data are discussed in § 3 and turbulence data in § 5. Some discussion is given in § 4 on what the mean-flow results represent in terms of the changing pattern in the mixing region. The boundaries of the mixing region are constructed from the mean velocity data and their changing position with changing exit conditions is discussed.

2. Apparatus and techniques

The arrangement of the air system is the same as that used in the earlier study (I). The subsonic and supersonic nozzles are specially contoured to give parallel flow at the exit and the design Mach number of the two supersonic nozzles is selected on the basis of schlieren flow pictures and the conditions which give an essentially shock-free flow. All the nozzles have an exit diameter of 51 mm.

The laser velocimeter system has also been discussed in some detail before (I). Various validation circuitry are incorporated in the system to eliminate double or missed counts in the acquisition of the individual velocity data points, and the analysis system is designed to remove erroneous biasing of the velocity histograms.

The total head probe is 3 mm in diameter and its measurements are calibrated against the plenum pressure. An iron–constantin thermocouple set within a 3·5 mm diameter sheath is used to measure the total temperature. It is first calibrated in ice and boiling water and checked against measurements made with a chromel–alumel thermocouple located in the plenum. The probes are mounted on the LV frame and, in traversing the jet, the probes are moved from point to point, remaining long enough at each point for the conditions to reach stability.

3. Mean-flow quantities

3.1. *Radial distributions*

(*a*) *Axial mean velocity.* Figure 2 shows radial distributions of the axial mean velocity for two Mach 0·5 jets: one being unheated and the other heated to an absolute static temperature (T_J) of 2·32 times that of the ambient (T_0). The velocity is normalized by the jet efflux velocity (U_J) and the radial position is given by the parameter $\eta^* = (r - r_{0.5})/x$, where $r_{0.5}$ refers to the position where the mean velocity is $0{\cdot}5U_J$. As was pointed out in I, this method of presenting the results proved to be most productive in our attempts to collapse the mean-velocity data over the jet flow field, and it was found that mean-velocity distributions as far downstream as two potential core lengths would fall on one universal curve. The present results show that not only isothermal jets but hot jets also produce results which have a tendency to collapse when plotted in this manner.

The main deviation of the two sets of curves is in the region between $\eta^* = 0$ to $-0{\cdot}08$, and an explanation for this may be found in figure 3, which shows the radial distributions of the Mach-number ratio (M/M_J), the static temperature-difference ratio [$\Delta T/\Delta T_J = (T - T_0)/(T_J - T_0)$], and velocity ratio ($U/U_J$) of a Mach 0·7 jet at $T_J/T_0 = 2{\cdot}32$. This graph is representative of results obtained over a range of exit Mach numbers ($M_J = 0{\cdot}5$ to $1{\cdot}4$).

The Mach-number distribution also represents the velocity distribution for an isothermal ($T_J/T_0 = 1$) jet, and it may be seen by comparison of the M/M_J and

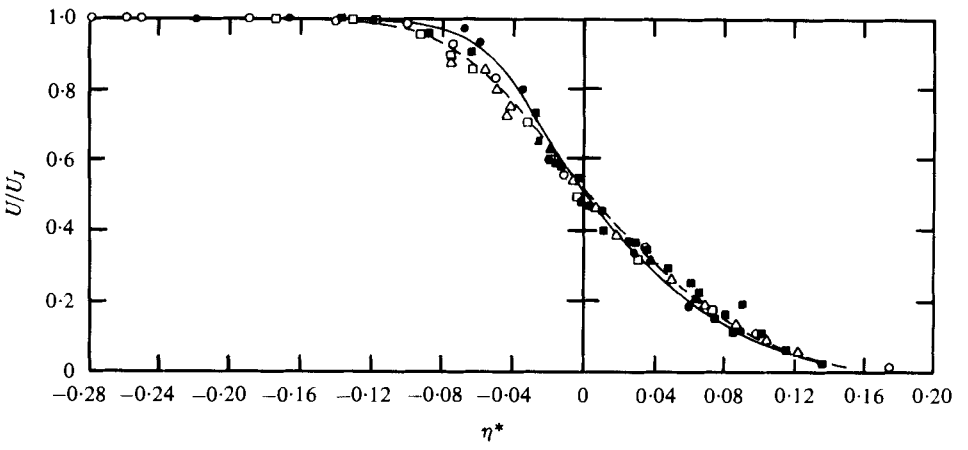

FIGURE 2. Radial distribution of the normalized axial mean velocity ($M_J = 0{\cdot}5$). $T_J/T_0 = 0{\cdot}95$ and 2·32 (solid symbols and full line). x/D: ○, 2; □, 4; △, 8.

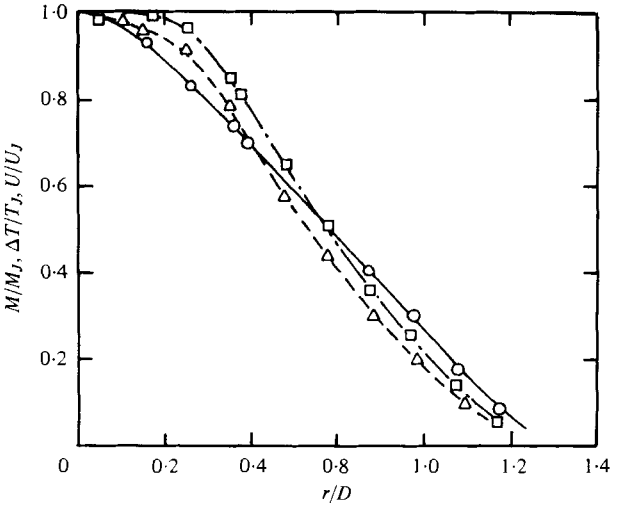

FIGURE 3. Radial distribution of: □, M/M_J; ○, $\Delta T/\Delta T_J$; △, U/U_J. ($M_J = 0{\cdot}7$, $T_J/T_0 = 2{\cdot}32$, $x/D = 4$).

U/U_J curves that the normalized velocity falls off more rapidly with radial distance for a heated jet. Distributions of the Mach-number ratio have been obtained for subsonic jets at varying exit static temperatures, and it is found that, for a given Mach number, heating the jet up to an exit temperature ratio of 2·32 results in no change to the distribution within the region up to $x/D = 4$. (At $x/D = 8$ the results tend to lie a little lower than those for an isothermal jet but not significantly so.) Since $U \sim MT^{\frac{1}{2}}$, it would seem that, in the initial region at least, the changes in the velocity distribution are caused by the non-uniformity in the temperature distribution. The more rapid fall in the normalized velocity associated with heated jets is therefore a result of the static temperature falling with radial distance from the jet axis as shown in the figure. The net effect is that the maximum gradient of the velocity distribution becomes greater with jet heating.

The effect of the non-uniform temperature distribution could also be observed from another perspective as shown in figure 4. It shows the radial distribution of the unnormalized mean velocity obtained with the LV at different jet-exit temperature ratios. Heating apparently raises the velocity in the inner region of the jet, leaving the outer region unaffected. As the temperature is raised the affected region extends further outward radially.

The locus of points at which heating begins to have an effect on the mean velocity is plotted in figure 5 for jets at Mach 0·5, 0·7 and 0·9. At a temperature ratio (T_J/T_0) of 1·5, the affected region (enclosed by the lines joining the open symbols) has a shape that is somewhat similar to that of the potential core. However, when the exit temperature is increased ($T_J/T_0 = 2{\cdot}32$), the region of influence grows with axial distance at first and subsequently contracts. The affected region apparently stretches downstream as the Mach number is increased, in harmony with the stretching of the jet (I).

It would seem therefore that the overall effect of heating the jet is to distort the mean velocity distribution from its unheated state and simultaneously cause a radial movement, in some cases, of the half-velocity point (figure 4). This results in normalized distributions, as shown in figure 2, which do not differ substantially from those of the corresponding unheated jet except in the specified region.

The slight deviation observed between the heated and unheated jet results indicate a higher maximum slope of the normalized velocity distribution for the heated jet, and if the spreading rate of the region is defined by $\delta_\eta = U_J/(\partial U/\partial \eta^*)_{\max}$ as in I, this would suggest that a hot jet has a smaller spreading rate than a cold jet.

The variation of the spreading rate (δ_η) with temperature ratio (T_J/T_0) is summarized in figure 6 for jets of varying Mach numbers (M_J). A difference may be seen between the results of subsonic and supersonic jets. With subsonic jets, initially heating the jet from T_J/T_0 1·0 to 1·5 produces a very small change in δ_η, but from $T_J/T_0 = 1{\cdot}5$ to 2·32, δ_η falls more noticeably. With supersonic jets the same behaviour is observed with initial heating but, as the temperature is raised further, δ_η *rises*. The curves seem to converge at about $T_J/T_0 = 2{\cdot}4$ and suggest that, at $M_J = 1{\cdot}0$, δ_η would probably not change significantly over the temperature range.

For temperature ratios of less than 2·4, the general tendency is for δ_η to fall with increasing Mach number. This trend is illustrated in figure 7 which shows the variation of δ_η with M_J for fixed values of T_J/T_0. The present experimental results are shown by the solid symbols. For $T_J/T_0 = 1{\cdot}0$ and 1·5, δ_η decreases monotonically with increasing M_J between Mach 0·3 and 1·4 and there is little distinction between them. The fall in δ_η with increasing M_J, however, does not continue without interruption. The trend appears to reverse for $T_J/T_0 = 1{\cdot}0$ and 1·5 at about $M_J = 1{\cdot}5$ and 1·3, respectively. Under these conditions the convection velocity of the large-scale structure in the mixing region ($U_c \approx 0{\cdot}7U_J$, see figure 13 of II) is in the order of the ambient speed of sound (a_0). Earlier schlieren pictures of jets issuing from different supersonic nozzles at different exit conditions reveal no outstanding feature when the convection velocity of the large-scale structure is supersonic. The reason for this upturn in value of δ_η is not clear at present and would have to be explored more fully. However, there appears to be a consistency in this result, and for $T_J/T_0 = 2{\cdot}32$ the turning point may be seen at about $M_J = 1{\cdot}0$ which would result in a convection velocity of about a_0 also.

The relative disposition of the two curves in the figure representing results at

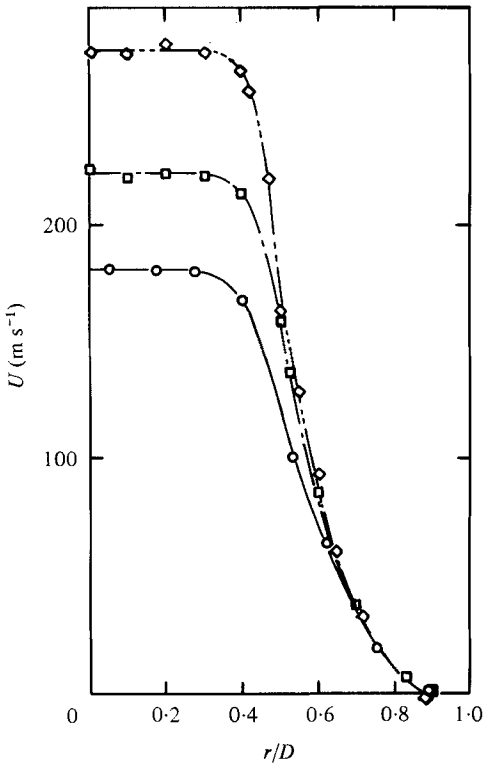

FIGURE 4. Radial distribution of the axial mean velocity. (M_J = 0·5, x/D = 2). T_J/T_0: ○, cold; □, 1·5; ◇, 2·32.

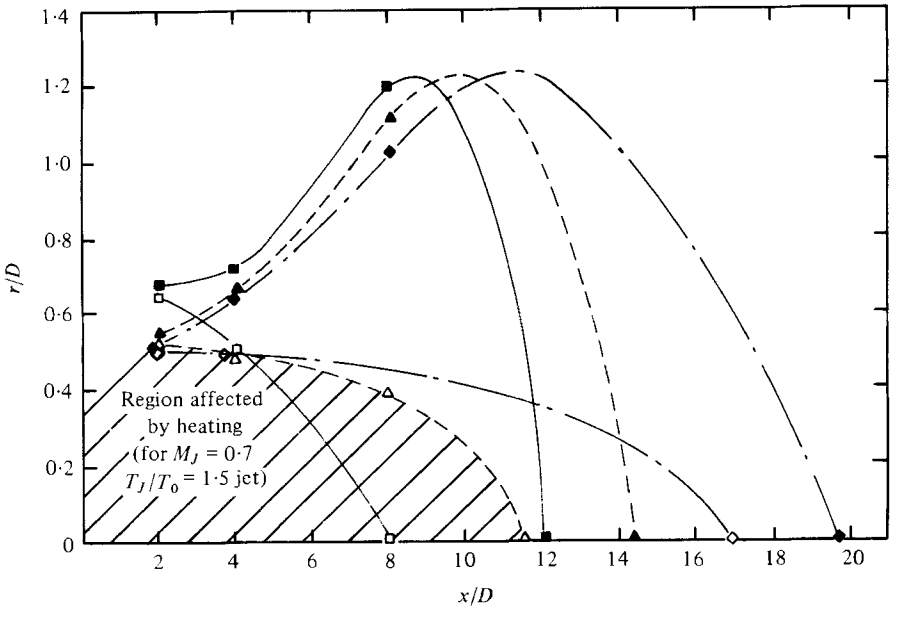

FIGURE 5. Physical plane showing approximate boundary of region affected by heating. T_J/T_0 = 1·5 and 2·32 (solid symbols). M_J: □, 0·5; △, 0·7; ◇, 0·9.

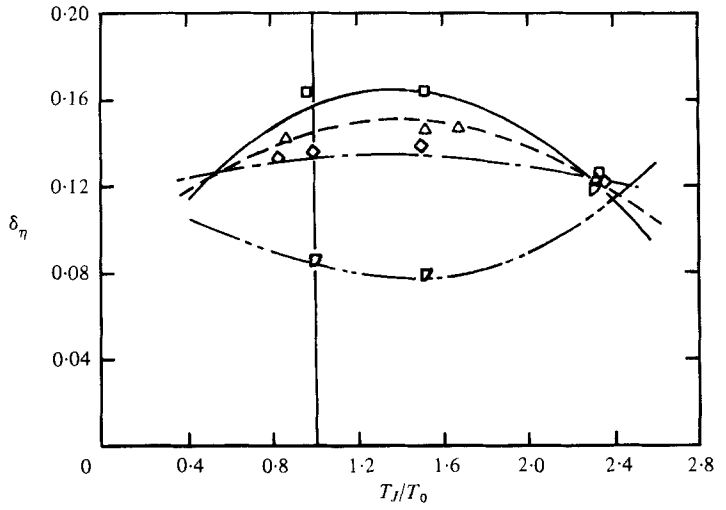

FIGURE 6. Variation of the spreading rate with temperature ratio. M_J: □, 0·5; △, 0·7; ◇, 0·9; ▽, 1·37. The lines are derived from equation (1).

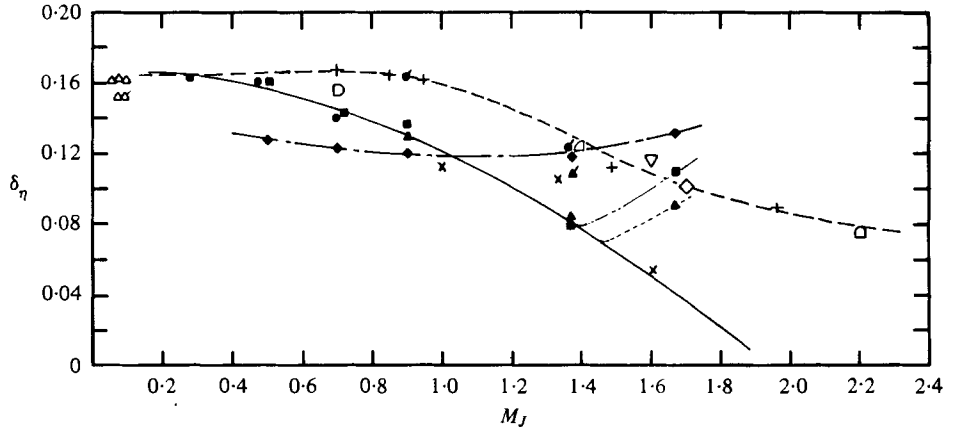

FIGURE 7. Variation of the spreading rate with Mach number. Present results T_J/T_0: ●, cold; ▲, 1·0; ■, 1·5; ◆, 2·32; flagged symbols refer to Pitot-tube results. △, Tollmien (1926), Liepmann (1947); ⧋, Reichardt (1942); ▽, Gooderum *et al.* (1949); ◇, Bershader & Pai (1950); ×, Cary (1954); ⧠, Crane (1957); ⧈, Johannesen (1959); +, Maydew & Reed (1963); ⧈, Eggers (1966).

$T_J/T_0 = 1{\cdot}0$ and $2{\cdot}32$, respectively, and the manner in which they cross, are reminiscent of corresponding curves showing the variation of the far-field noise intensity with U_J/a_0. At 90° to the jet axis where the noise generated by the flow is uncomplicated by refraction and other acoustic–mean-flow interaction effects, Tanna (1977, figure 3) has found the noise intensity generally to vary as $(U_J/a_0)^n$. The value of n decreased with the increase of T_J/T_0 from 1·0 to 2·3 and 3·4, and the curves representing results at these temperature ratios intersected each other. Since δ_η is inversely proportional to the maximum slope of the mean velocity distribution (or the maximum shear), it may

be inferred that there is a direct relationship between the far-field noise intensity and the maximum shear in the jet shear layer.

Figure 7 also shows results obtained in cold jets by other investigators (compiled by Birch & Eggers 1972). As in the present results for isothermal jets, the value of δ_η generally falls with increasing M_J; but except for Cary's (1954), which were obtained with a non-intrusive instrument, these earlier results tend to be somewhat higher at $M_J > 0{\cdot}3$, the difference increasing as M_J is increased. The earlier results had been obtained with a Pitot probe and, to verify that the difference was not due to a deviation of the present jet structure from that of the earlier jets, measurements were repeated in the present jet (I) using a Pitot probe. An isothermal jet at $M_J = 1{\cdot}37$ was chosen for this purpose, and it was found that indeed the value of δ_η (flagged solid triangle) determined from these results was higher than that obtained from corresponding LV measurements and approached those of other investigators. In the present study, the Pitot measurements are extended to include a couple of cold jets (flagged solid circles) and in these cases the data points lie right on the curve passing through the data of earlier investigators.

Efforts to discover the reasons for this discrepancy are still in progress and preliminary results indicate that radial distributions of the velocity measured with an LV become distorted also and approach those obtained with Pitot probes when a Pitot tube is mounted behind the measurement volume of the LV. The distance between the measurement volume and the nose of the probe does not appear to be a critical factor in this change. The distributions of the turbulence intensity on diametrically opposite shear layers are also seen to move closer to the jet axis. It appears therefore that the presence of the probe does alter the jet structure to some extent, but the full details of this change and how it is brought about is still unclear at present.

An empirical expression is derived based on the present results to describe the variation of δ_η with T_J/T_0 and M_J and is given by

$$\delta_\eta = 0{\cdot}177\{(1-0{\cdot}294M_J^2)[1+0{\cdot}5(M_J^2-1)(T_J/T_0-1{\cdot}4)^2]\}. \tag{1}$$

This may also be expressed in terms of the Görtler spreading parameter (σ) by using Korst & Chow's (1962) relationship of $\sigma\delta_\eta = \sqrt{\pi}$. Curves representing the above expression are drawn for $M_J = 0{\cdot}5$, $0{\cdot}7$, $0{\cdot}9$ and $1{\cdot}37$ in figure 6.

It was found (I) that, by plotting radial distributions of the mean velocity in terms of $\sigma\eta^*$, data of all isothermal jets in the range from Mach 0·3 to 1·4 collapsed on a universal curve. A similar attempt is made here with the hot and cold jet results and the data (including the isothermal data) similarly collapse on a curve in as compact a manner as that shown in figure 22 of I. The curve may reasonably be represented by the Görtler error-function profile: $U/U_J = 0{\cdot}5[1-\mathrm{erf}(\sigma\eta^*)]$.

(*b*) *Temperature difference ratio.* Although temperature distributions only form an adjunct to our primary interest which is the velocity distributions, there are nevertheless some interesting observations concerning the temperature distributions which may be worth pointing out. Figure 8 shows the static temperature distributions plotted in terms of the temperature difference ratio (defined earlier for figure 3) and $\eta_t^* = (r-r_{0{\cdot}5t})/x$, $r_{0{\cdot}5t}$ being the radius where $\Delta T/\Delta T_J = 0{\cdot}5$. The results for the Mach 0·5 and 0·7 jets apparently fall close to each other, but a careful comparison of the two results suggests that the maximum gradient of the distribution for the Mach 0·7 jet may be a little higher. This would be in agreement with the trend observed

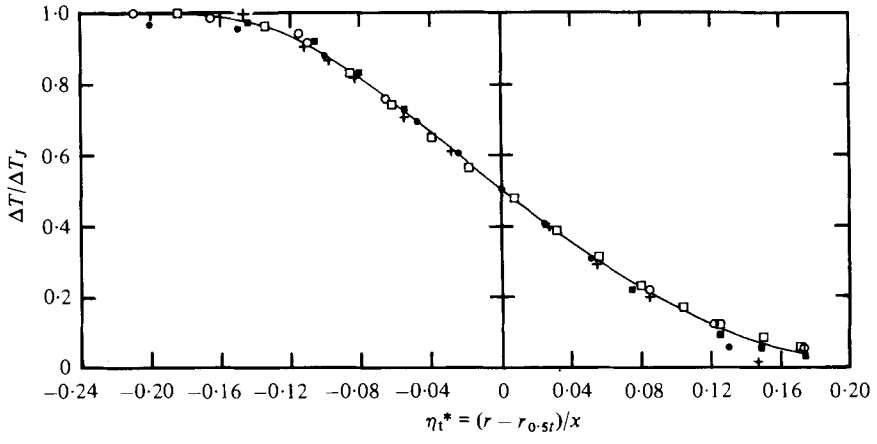

FIGURE 8. Radial distribution of the static temperature difference ratio. M_J = 0·5 and 0·7 (solid symbols). x/D: ○, 2; □, 4. + Yakovlevskiy (Abramovich 1963).

in velocity distributions (I) which suggests that the jet structure stretches and the shear layer narrows when the jet-exit Mach number is increased. Yakovlevskiy's results (Abramovich 1963) obtained over a range of Mach numbers of 0·1 to 0·4 are also shown and compare well with present data.

The maximum slope of these curves is in general lower than that of corresponding velocity distributions, suggesting that the thermal shear layer is spread over a larger cross-section of the jet than the velocity shear layer. This would also be in agreement with the results of Corrsin & Kistler (1955) and Yakovlevskiy. If a spreading rate is defined for the temperature distribution ($\delta_{\eta t}$) as for the velocity distribution (δ_η), the relationship between them is given by

$$\delta_{\eta t} = 1{\cdot}45\delta_\eta \tag{2}$$

based on Pitot measurements of the mean-velocity distributions. This would agree with Batt's (1977) constant of 1·41. The extent of the influence of a temperature probe situated in the flow is not assessed at this juncture but since both $\delta_{\eta t}$ and δ_η are based on results obtained with probes of nearly the same size the two quantities may be considered to be compatible, and the comparison probably valid generally.

An error-function-type profile is drawn through the data and there is very good agreement between them even in the region around $\eta_t^* = +0{\cdot}1$, where velocity data have been known to deviate somewhat (figure 22 of I).

The half-temperature difference point ($r_{0\cdot5t}$) generally lies outside of the half-velocity point ($r_{0\cdot5}$) and, as the axial distance from the nozzle is increased, the separation becomes less. This is observed in both the Mach 0·5 and 0·7 jets.

Abramovich (1963) has suggested that the *total* and *static* temperature distributions may be represented by the same expression. Figure 9 shows the distributions of the total and static temperature difference ratios at two axial stations and it is evident that there is a small deviation between the corresponding distributions: the maximum slope of the distribution for the *total* temperature difference ratio being higher than that for the *static* temperature difference ratio.

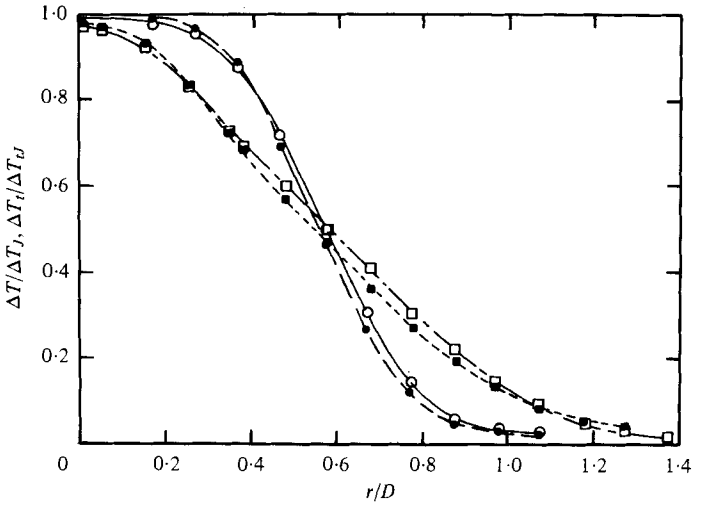

FIGURE 9. Radial distribution of temperature difference ratios: $\Delta T/\Delta T_J$ and $\Delta T_t/\Delta T_{tJ}$ (solid symbols). ($M_J = 0{\cdot}7$, $T_J/T_0 = 2{\cdot}32$). x/D: ○, 2; □, 4.

3.2. *Axial distributions*

(*a*) *Mean velocity.* The effect of Mach number on the distribution of the mean velocity along the jet centre-line was studied in some detail in I for isothermal jets. The results showed trends which have been known for some time (Birch & Eggers 1972), i.e. that the distributions move downstream as the Mach number is increased. The effects of heating have, however, not been as well documented.

From a systematic study of heated jets at fixed Mach numbers, it is found that heating causes the distributions to move upstream, but that the movement apparently stops beyond an exit temperature ratio of about 1·5. Typically, for all Mach numbers considered, the distributions move in almost equal steps upstream from a cold jet to jets at $T_J/T_0 = 1{\cdot}0$ and 1·5, respectively. Heating to $T_J/T_0 = 2{\cdot}32$ produces no further change in the distribution (figure 7 of Lau 1978). It would seem therefore that heating causes the jet potential core to contract until about $T_J/T_0 = 1{\cdot}5$ when the potential core reaches a limiting state. This contrasts with the trends observed with regard to the spreading rate (δ_η) of the shear layer, where initial heating from $T_J/T_0 = 1{\cdot}0$ to about 1·5 evoked no change, and it was only as T_J/T_0 was increased from 1·5 to 2·32 that changes were observed. Moreover, the spreading rate was seen to decrease with heating. It is clear therefore that the reduction in the potential core length with heating is not associated with an increase in the spread of the mixing region. Apparently the shear layer rotates towards the jet axis when heat is applied to the jet.

(*b*) *Universal curve for centre-line distributions.* It was found with isothermal jets that, although the centre-line distributions moved with changing M_J, they could be reduced to a single curve by plotting the normalized velocity distributions in terms of x/x_c, x_c being the respective potential core length of the jet. Moreover the curve could be represented to a good degree of accuracy by the Kleinstein–Witze formula [equation (4) of I]: $U_a/U_J = 1 - \exp\{\alpha/(1 - x/x_c)\}$.

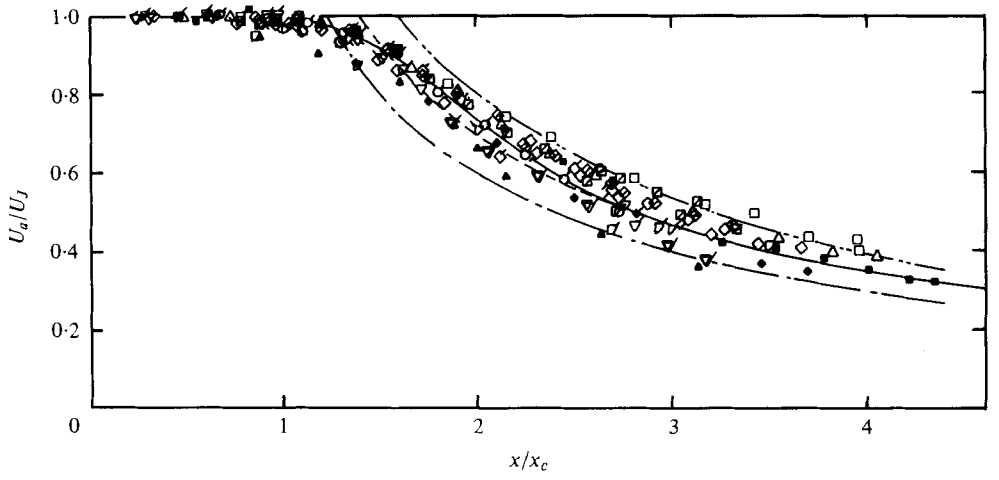

FIGURE 10. Universal axial distribution of mean velocity. ——, Kleinstein–Witze formula (see I, $\alpha = 1{\cdot}35$). — — —, asymptotic formula with $\alpha = 1{\cdot}2$; - - - -, $\alpha = 1{\cdot}4$; — — — —, $\alpha = 1{\cdot}6$.

	M_J					
T_J/T_0	0·28	0·5	0·7	0·9	1·37	1·67
Cold	⊘	⊠	△	◇	—	—
1·00	—	□	—	◇	▱	▽
1·50	—	□	△	◇	▱	▽
2·32	—	■	▲	◆	▰	▼

A similar exercise is carried out with the results of heated and cold jets. The data from the eighteen test conditions also tend to collect in one narrow band (figure 10) but there is more scatter here than in the corresponding results for isothermal jets alone (figure 16 of I) or in the universal plot of radial distributions. A Kleinstein–Witze curve drawn through the middle of the data points would have a value of α of 1·35 as for the isothermal jet results.

Traditionally, it has been maintained that far downstream of the potential core, where the jet has had the opportunity to become 'fully developed', the velocity on the centre-line varies as $1/x$. Indeed, for very large x, the Kleinstein–Witze formula reduces to $\alpha x_c/x$. It is found that in this case a more appropriate value for α would be 1·4. There is good agreement between this asymptotic curve and the experimental data beginning from about $x = 2{\cdot}5x_c$, and based on Wyganski & Fiedler's (1969) results, it would seem that the agreement extends to about $x = 13x_c$.

The good collapse of the data of jets at varying M_J and T_J/T_0 implies a value of α which is unaffected by jet conditions. This assumption is also implicit in the results of both Witze and Kleinstein (Witze 1974) who took the value of 1·43. However, this is apparently not exactly true. For instance, figure 11 shows a plot of $1/\alpha(T_J/T_0)^{0{\cdot}2}$ against M_J and it clearly reveals a slow variation of α with M_J and T_J/T_0. Kleinstein's and Witze's value of α is also indicated in the figure, and lies close to the average of the extreme values on the graph. It would seem that, depending on the range of Mach numbers considered, the average value of α could be different; and the dissimilarity between Kleinstein's and Witze's value of α and the present average could be traced

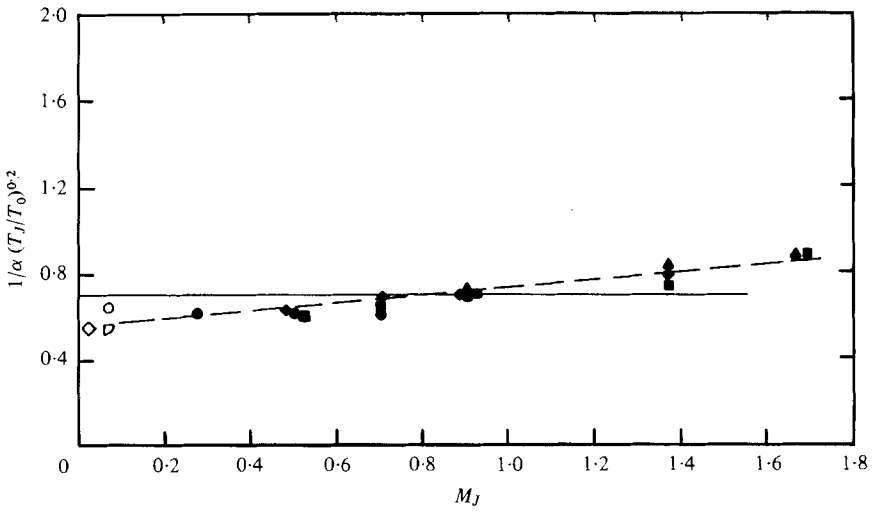

FIGURE 11. $1/\alpha\,(T_J/T_0)^{0\cdot2}$ *vs.* M_J. T_J/T_0: ●, cold; ▲, 1·0; ■, 1·5; ◆, 2·32 (present results). ○, cold; ▽, 2·06 (Corrsin & Uberoi). ◇, cold (Szablewski). ——, Kleinstein (Witze 1974).

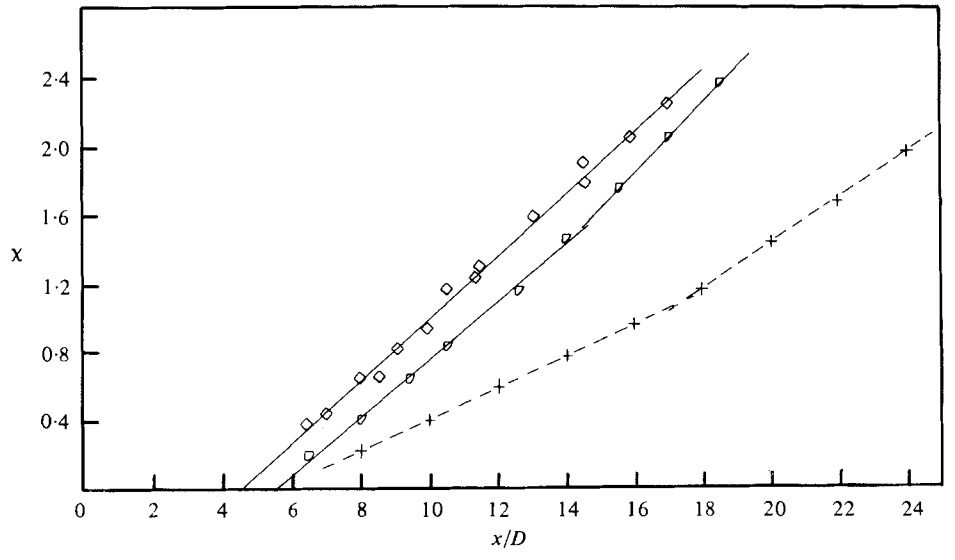

FIGURE 12. Axial distribution of the mean velocity parameter χ. ($T_J/T_0 = 2{\cdot}32$). M_J: ◇, 0·9; ▽, 1·37. +, Eggers (1966) (abscissa scale is $(T_J/T_0)^{0\cdot5}\,x/D$).

to this situation. This could also help to explain the apparent scatter in the plot of figure 10.

Before leaving the discussion of the Kleinstein–Witze formula, it should be pointed out that, although the U_a/U_J *vs.* x/D curves for supersonic jets appear to be smooth and do not differ greatly in appearance from curves for subsonic jets, the decay in the centre-line velocity actually goes through two stages, one within the region where the flow is still supersonic and the other downstream of the sonic point. When the results

are plotted in terms of the mean velocity parameter $\chi(=1/\{\ln(1-U_a/U_J\})$, the separation between the two regions becomes more apparent (figure 12). The data for the subsonic jet form one straight line, but those for the supersonic jet tend to lie on two straight lines which intersect at about the location where the Mach number is 1·0. Since the slope is smaller for the supersonic region, this would indicate that the rate of decay in the centre-line mean velocity is more gradual in the supersonic region of the jet. Eggers' (1966) results for an unheated jet at $M_J = 2{\cdot}2$ are also shown, and the same trend is present. (Note: To ensure that the essential features of the data would appear in the same figure, Eggers' results have been plotted with the abscissa scale equal to $(T_J/T_0)^{0{\cdot}5}x/D$.)

Occasionally, the potential-core length (x_c) is obtained by the extrapolation of the χ *vs.* x/D results to the abscissa and, when this happens, a failure to recognize that there are actually two separate slopes in the plots for supersonic jets could conceivably lead to errors in the determination of x_c in supersonic jets. In the present results, therefore, a clear distinction is made between the data points for the supersonic and subsonic regions and only the supersonic data are used in the extrapolation to obtain x_c.

(*c*) *Potential-core length.* From the foregoing, it is clear that the jet structure undergoes stretching or contraction depending on whether the exit Mach number or the exit temperature ratio is increased, and the potential-core length affords a means of quantifying these effects. Figure 13 shows the variation of x_c/D with M_J and T_J/T_0 and represents an expanded version of a similar plot shown in I. The solid symbols show the present results and it may be seen that for isothermal jets the earlier empirical equation [equation (8) in I] holds true up to about Mach 1·5 only. Beyond that the data tend to rise above the curve. Heating the jet to $T_J/T_0 = 1{\cdot}5$ and 2·32 reduces x_c/D and the results run almost parallel to those for isothermal jets.

The effect of jet heating was considered earlier by Witze (1974) who suggested that x_c/D would vary linearly with $(T_J/T_0)^{-0{\cdot}28}$ for subsonic jets and $(T_J/T_0)^{-0{\cdot}5}$ for supersonic jets. The present results, however, indicate the same relationship for both subsonic and supersonic jets. Instead, a difference is found between heated and unheated jets. For heated jets (included in this group are isothermal jets), x_c/D varies as $(T_J/T_0)^{-0{\cdot}2}$ and for unheated jets it varies as $(T_J/T_0)^{-0{\cdot}5}$. These differences may help partly to explain why Witze's prediction for isothermal supersonic jets was found to be inaccurate (I).

Another explanation may be found in the difference in the type of instrument used. To assess the contribution from this, Pitot measurements are carried out in the present jet. It is found that at low Mach numbers Pitot probe and LV data do not differ, but at high Mach numbers LV results of x_c are higher than those obtained with a Pitot probe. For instance at $M_J = 0{\cdot}9$, the LV gives a value of $5{\cdot}8D$ while the Pitot probe gives a valueof $4{\cdot}7D$. This discrepancy seems to be related to a phenomenon discussed earlier concerning differences in radial distributions depending on whether a probe is placed in the flow, and will be the subject of a subsequent paper.

(*d*) *Total and static temperature difference ratio.* Centre-line distributions of the total and static temperature difference ratios differ by a small amount in much the same way as the radial distributions. As the Mach number is increased, the distributions move downstream, conforming to the stretching of the jet pattern.

These distributions begin to decay significantly earlier than velocity distributions,

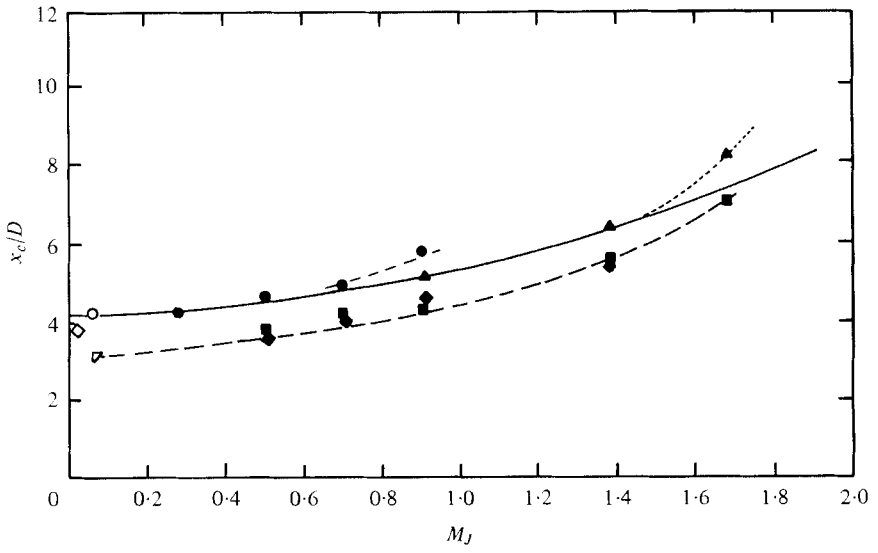

FIGURE 13. Variation of the potential-core length with Mach number. T_J/T_0: ●, cold; ▲, 1·0; ■, 1·5; ◆, 2·32 (present results). ○, cold; ▽, 2·06 (Corrsin & Uberoi). ◇, cold (Szablewski, Faris). ——, equation (8) of I.

suggesting that the potential core of the thermal flow field (x_{ct}) is shorter than that of the velocity flow field (x_c). At Mach 0·5, x_{ct} is about $0{\cdot}077x_c$. Since the Mach number in the initial region remains unchanged with jet heating (see § 3.1 *a*), the velocity is dependent on the local temperature, and it is clear why the potential core of the velocity field would contract when the jet is heated.

4. Changes to the boundaries of the mixing region

The various distributions of the mean quantities studied in the previous section clearly show that the simplistic view offered before by other investigators that the potential core reduces in size purely due to the increasing spreading rate of the mixing region is no longer adequate. Instead, it appears that the mixing region may undergo two kinds of transformation: (*a*) it may change its spreading rate, as has been assumed previously, and (*b*) it may rotate towards or away from the jet axis. In order to separate these two effects, an attempt is made in this section to reconstruct the boundaries of the mixing region from the mean-flow distributions and study their movement when the jet conditions are changed.

4.1. *Mixing-region boundaries*

The mixing region has one boundary which it shares with the potential core and another with the entrainment region, and based on the linear growth of the shear layer (evidenced by the good collapse of the data when the mean velocity distributions are plotted in terms of $\eta^* \sim 1/x$), it is expected to be bounded by two straight lines. Therefore, only two points are needed to define each boundary.

In the case of the boundary on the potential-core side of the mixing layer, the point

at $x = x_c$ on the jet centre-line could be one of them. The other could be a point in the jet-exit plane at about $r/D = 0{\cdot}55$, which is the approximate position of peak turbulence level close to the nozzle.

The latter could also serve as one of the points on the outer boundary, and therefore any rotation of the mixing region may be thought to occur about this pivotal point. The second point on the boundary may be determined from the available data on the spreading rate of the mixing layer, given the location of the inner boundary. At $x = x_c$, the distance of the outer boundary from the jet axis would be equal to the thickness of the shear layer at this point or $x_c\delta_1$, where $\delta_1 = \eta^*_{0{\cdot}01} - \eta^*_{0{\cdot}99}$. On the basis of a Görtler error-function-type profile (I) it may be shown that $\delta_1 = 1{\cdot}85\delta_\eta$. Therefore, the distance of the outer boundary at the end of the potential core (Δ_c) is given by $1{\cdot}85x_c\,\delta_\eta$, which may be determined from figures 7 and 13.

The relationship between Δ_c/D and x_c/D is shown in figure 14 for jets of varying exit conditions. The figure, in essence, represents the physical plane of the top half of the jet, and the data points show how the outer boundary moves with changes in the jet-exit Mach number and temperature. This concept is illustrated by the straight lines drawn, for the jet emerging at Mach 0·3 and temperature ratio of 1·0, to represent the inner and outer boundaries.

For clarity, the ordinate scale of the figure (representing the radial dimension) is made five times larger than the abscissa scale (the axial dimension) and to distinguish the special cases where the eddies convect at speeds greater than the ambient speed of sound (please see figure 7), a circle is placed around those data points which have these jet conditions.

The data points fall along lines of constant exit (*a*) Mach number, (*b*) temperature ratio, and (*c*) velocity and, if the special cases are excluded, the points form a fairly consistent grid pattern with an apex at **A**.

Tracing firstly the changes along a $T_J/T_0 = 1{\cdot}0$ line from **A**, it may be seen that, as the Mach number is increased, the outer boundary rotates inwardly. At the same time, the potential-core length is increasing. Therefore the inner boundary is rotating outwardly. The more obvious effect is that the fan representing the mixing layer becomes contracted. However, the angular displacement of the outer boundary is greater than that of the inner boundary so that associated with the contraction there is also a rotation of the mixing layer towards the jet axis as the Mach number is increased. The same behaviour is evident in heated jets at $T_J/T_0 = 1{\cdot}5$ although to a lesser extent. For jets heated to $T_J/T_0 = 2{\cdot}32$, however, the situation is somewhat different. Both the outer and inner boundaries rotate outwardly and the net effect is that the whole mixing layer rotates with marginal changes in the width of the layer.

Considering next the variations along constant-Mach-number lines, $M_J = 0{\cdot}5$ for example, it may be seen that both boundaries now rotate towards the jet axis. The movement of the inner boundary becomes progressively less as the temperature ratio is raised. Since the outer boundary is displaced through a larger angle than the inner boundary, the overall effect is a thinning of the mixing layer as it rotates toward the jet axis. These trends were outlined in figure 1 of II, which showed (*a*) the original boundaries of a low-speed unheated jet; (*b*) the new boundaries as the jet Mach number was increased while the temperature ratio (T_J/T_0) remained at $T_J/T_0 = 1{\cdot}0$ or 1·5; and (*c*) the new boundaries as the temperature ratio was increased with the Mach number remaining constant.

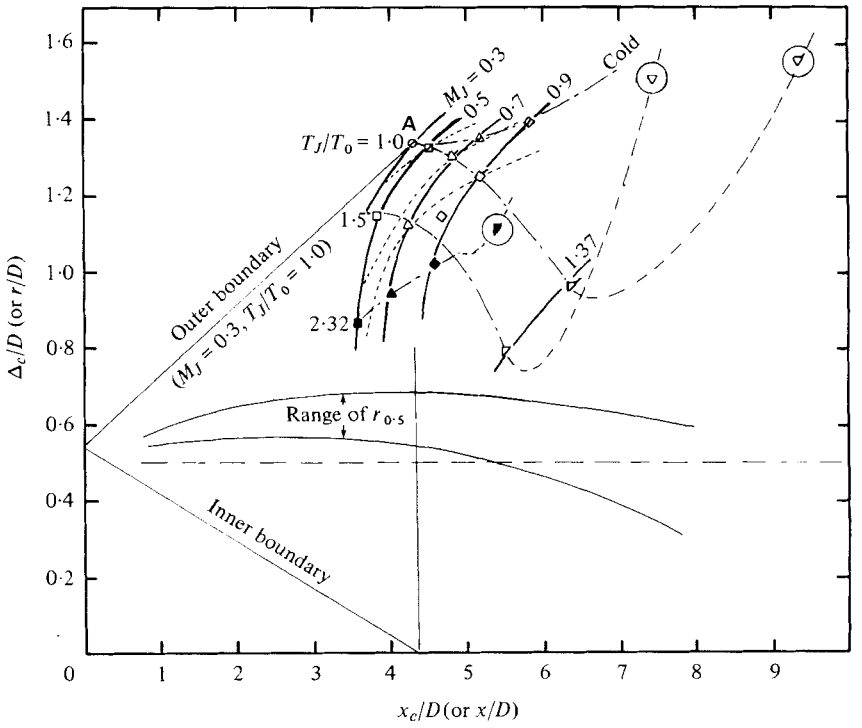

FIGURE 14. Half-plane of jet: Δ_c/D *vs.* x_c/D. ——, constant M_J; — — —, constant T_J/T_0; – – – –, constant U_J/a_0.

4.2. *Displacement of the half-velocity point*

The rotation of the mixing layer is reflected in the displacement of the loci of half-velocity points ($r_{0{\cdot}5}$). For instance in figure 15(*a*) which shows axial distributions of $r_{0{\cdot}5}/D$ for jets at a constant exit temperature ratio ($T_J/T_0 = 1{\cdot}0$) and varying exit Mach numbers, the curves move progressively inwards similarly to the trend suggested by the rotation of the mixing-layer boundaries. It is significant that the data points shown here form curves with small curvatures rather than straight lines, which might suggest that the boundaries are actually not straight lines but curves which bend slightly towards the jet axis.

Similar curves of $r_{0{\cdot}5}/D$ *vs.* x/D are drawn in figure 15(*b*) for jets at a constant Mach number and increasing temperature ratio. The curves move with increasing temperature ratio, signifying once again an inward movement of the mixing layer. It may also be noted that the rate of movement of the curves is greater here than that shown in figure 15(*a*), thus suggesting that the rotation of the mixing region is affected more by raising the jet-exit temperature ratio than by increasing the jet-exit Mach number in the range of conditions explored.

5. Fluctuating velocities

Although the LV in its most fundamental form is able to provide results of the mean and fluctuating velocities with gross features which follow hot-wire measurements (see § 1; I), the magnitudes of the turbulence intensity tend to be significantly higher

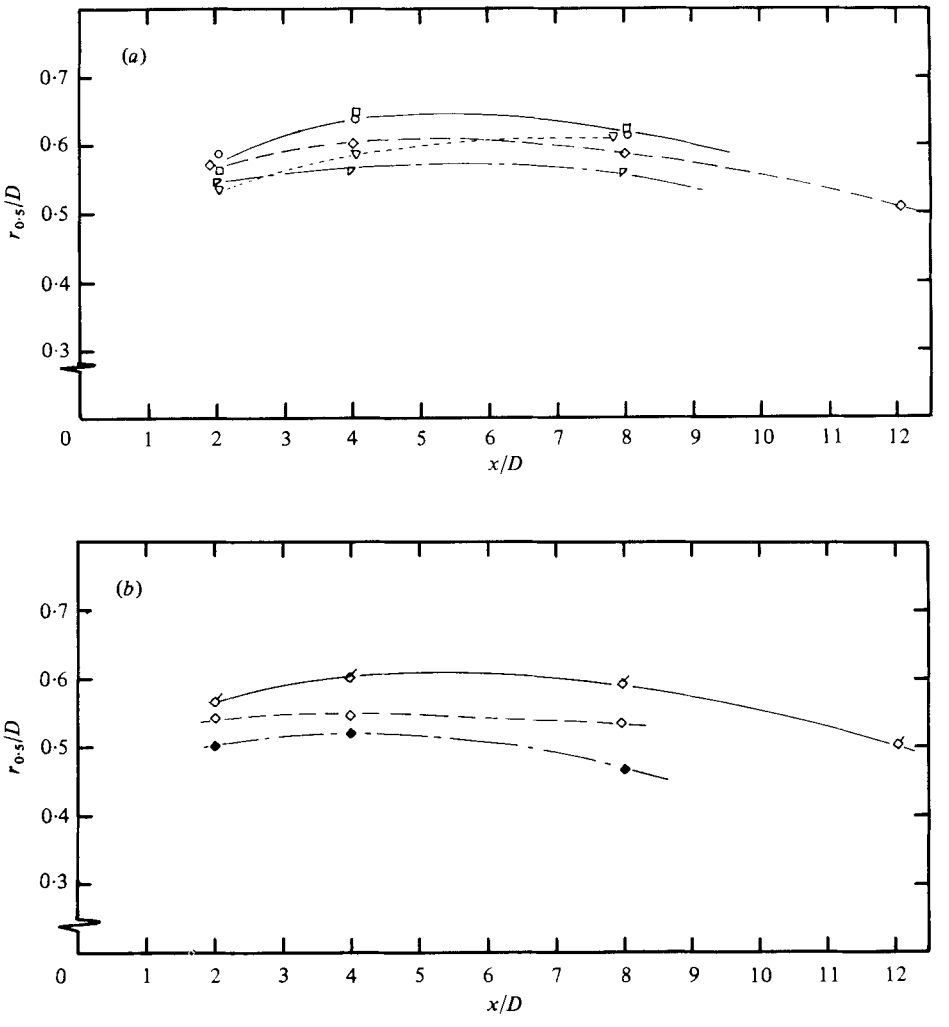

FIGURE 15. Axial distribution of the half-velocity point. (*a*) At constant temperature ratio $T_J/T_0 = 1{\cdot}0$. M_J: ○, 0·28; □, 0·5; ◇, 0·9; ▱, 1·37; ▽, 1·67. (*b*) At constant Mach number $M_J = 0{\cdot}9$. T_J/T_0: ◇, 1·0; ◇, 1·5; ◆, 2·32.

at some locations. Considerable effort has gone into the identification of this discrepancy, which apparently is caused by an inherent noise component in the photomultiplier signal due to the photon nature of light and the photon-averaging process involved in burst-counter-type LV systems. Specific methods have been devised to correct the turbulence reading (Whiffen *et al.* 1979; II) or eliminate the influence of the noise at the initial processing (Lau *et al.* 1981), and it is possible now to obtain data of turbulence which compare identically with corresponding hot-wire data. The methods work satisfactorily over the full Mach number range and an interesting outcome of these studies has been that a graph showing the relationship between the corrected and uncorrected local turbulence intensities have the data points lying on one straight line irrespective of the jet condition or the laser light condition when the data were

taken (Lau *et al.* 1981). Another relevant point is that results of covariances, such as those obtained by correlating data emanating from two separated photomultiplier tubes, are unaffected by the noise because the noise from the separate photomultiplier tubes is uncorrelated (II).

5.1. *Radial distributions*

Figures 16, 17 and 18 show the radial distributions of the axial ($\tilde{u}/U_J$) and radial ($\tilde{v}/V_J$) turbulence intensities and the covariance $\overline{u'v'}/U_J^2$, respectively, for a heated Mach 0·9 jet. The magnitudes of the turbulence intensities have been corrected by one of the methods mentioned above.

Typically, the radial distributions all show a peak close to $\eta^* = 0$, with the peak value falling with axial distance from the nozzle. As with isothermal jets (I), the peak values of $\tilde{v}/U_J$ are about two-thirds to three-quarters of the corresponding peak values of $\tilde{u}/U_J$. Variations due to the spreading of the shear layer are taken care of, as for the mean velocity results, by the expediency of plotting the distributions in terms of η^*, but the curves still do not collapse because the peak intensities are not maintained constant with axial position (I).

Another observation is that the peaks are not all located exactly at $\eta^* = 0$ or even at a fixed value of η^*. This is quite a different situation from the results of isothermal jets where all the peaks lie esssentially at $\eta^* = 0$ (I). It would seem therefore that the coincidence between the peak turbulence and half-velocity points observed in isothermal jets is not a universal character of jets. Moreover the positions of the peaks are such that it is not possible to identify the peak turbulence with any other particular characteristic of the mean velocity distribution (e.g. the position of maximum mean velocity gradient).

Figure 19 shows the radial distributions of the axial turbulence intensity for jets of varying exit Mach number and temperature ratio. The radial position is given in terms of $\sigma\eta^{**}$ which is referred to the position of the peak turbulence level rather than the half-mean-velocity point, and the turbulence level is normalized by the peak values ($\tilde{u}_p$) of the corresponding curves. The data points do not collapse as well as those of the mean velocity in a similar plot, but tend to gather together into a fairly narrow band. A curve of the form $\tilde{u}/\tilde{u}_p = \exp[-0{\cdot}70(\sigma\eta^{**})^2]$ is also shown in the figure and may as a first approximation be used to describe a universal distribution of the turbulence.

Distributions of peak turbulence intensity with x/D were presented briefly in I and not much could be mentioned about them. However with the availability of more data as a result of the expanded test programme in the present study, a pattern is beginning to emerge concerning these distributions which may provide insights into the changing structure of the jet as it convects downstream.

Figure 20 shows a family of these distributions for isothermal jets at varying Mach numbers. Taking the Mach 0·3 and 0·5 results first, it may be seen that $\tilde{u}_p/U_J$ falls gradually. This gradual fall apparently does not continue indefinitely downstream, and in figure 21, which shows these data and those of Wygnanski & Fiedler's (1969) plotted in terms of the reciprocal of $\tilde{u}_p/U_J$ there is an abrupt change in slope at about $x/D = 10$ and another at $x/D = 45$. The first point is located at about 2·3 times the potential core length from the nozzle exit plane and Wygnanski & Fiedler's data suggest that between $x/D = 10$ and 35 the variation of $\tilde{u}_p/U_J$ would be given by $\tilde{u}_p/U_J = 1{\cdot}55D/x$.

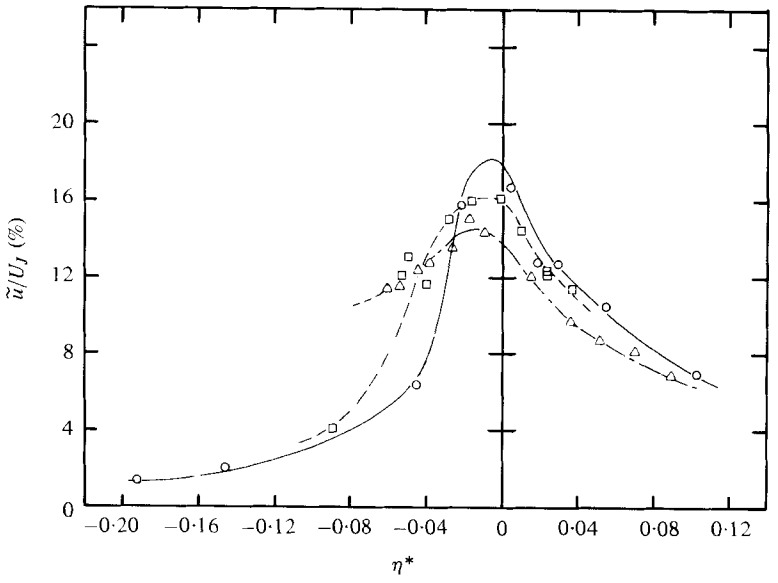

FIGURE 16. Radial distribution of the axial turbulence intensity ($\tilde{u}/U_J$). (M_J = 0·9, T_J/T_0 = 2·32). x/D: ○, 2; □, 4; △, 8.

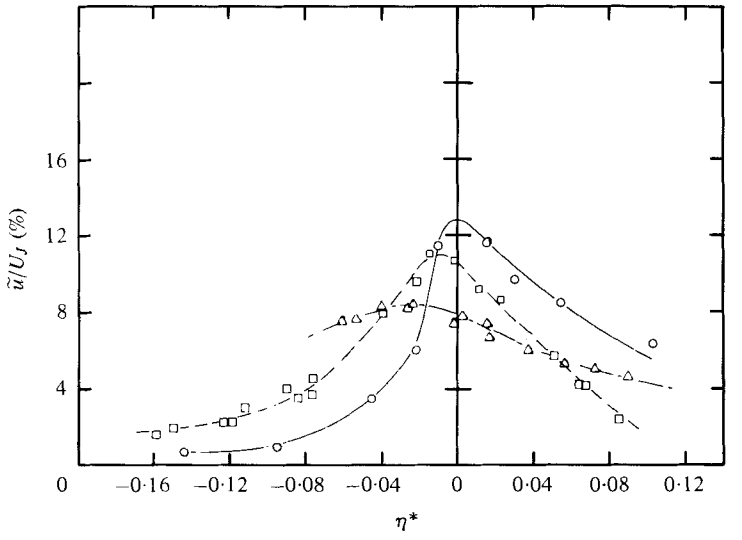

FIGURE 17. Radial distribution of the radial turbulence intensity ($\tilde{v}/U_J$). (M_J = 0·9, T_J/T_0 = 2·32). x/D: ○, 2; □, 4; △, 8.

These trends are confirmed in the Mach 0·9 results. Up to about $x = 13D$ or $2{\cdot}5x_c$, the fall is very gradual but, downstream of that, the $1/x$ fall is evident and a curve given by $1{\cdot}63D/x$ passes through the data point at $x/D = 16$. The Mach 1·37 data show similar tendencies and, based on the above trends, the significant change in slope is expected to occur at about $x/D = 16$. The Mach 1·67 data apparently follow

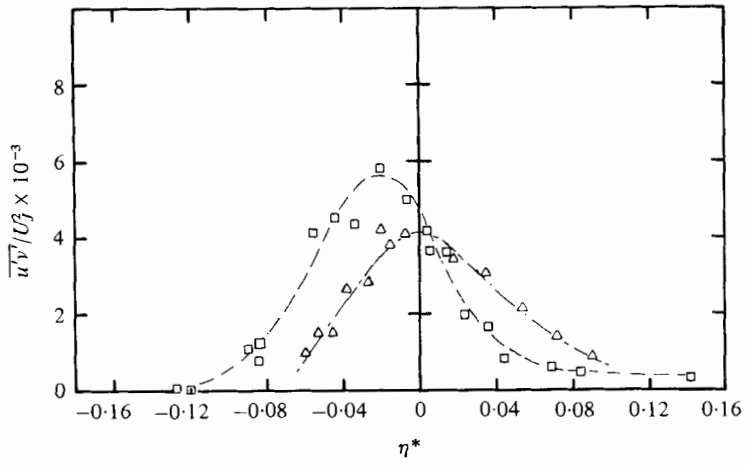

FIGURE 18. Radial distribution of the covariance $\overline{(u'v'/U_J^2)}$ ($M_J = 0{\cdot}9$, $T_J/T_0 = 2{\cdot}32$). x/D: □, 4; △, 8.

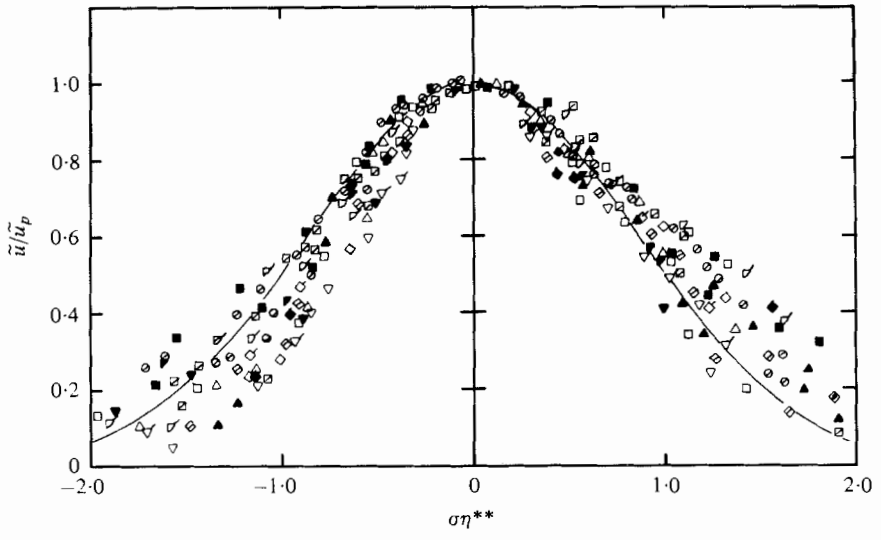

FIGURE 19. Universal radial distribution of the axial turbulence intensity (see legend in figure 10). ——, exp $[-0{\cdot}70(\sigma\eta^{**})^2]$.

a different trend and, between $x/D = 2$ and 8, the peak turbulence intensity rises gradually instead. Therefore, the trends observed earlier extend only up to a jet Mach number of about 1·4.

The abrupt change in the decay of $\tilde{u}_p/U_J$ at about twice the potential-core length would seem to suggest a possible change in the structure of the mixing region at about this point. It may be recalled that the mean velocity distributions also undergo a change in behaviour at this general location (I). These observations may be explained in the context of a two-component model of the mixing region proposed by Lau (1979). One component lies on the potential-core side of the mixing region and converges on the jet axis at about two potential-core lengths downstream of the nozzle exit plane

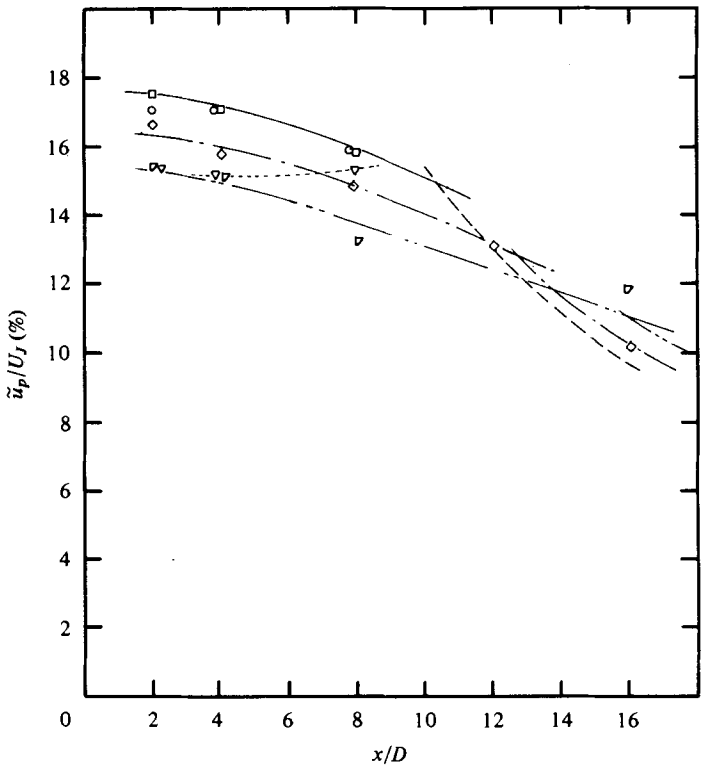

FIGURE 20. Axial distribution of the peak axial turbulence intensity. ($T_J/T_0 = 1{\cdot}0$.) M_J: ○, 0·28; □, 0·5; ◇, 0·9; ▽, 1·37; ▽, 1·67. The lines except for $M_J = 1{\cdot}67$ are derived from equations (3) and (4).

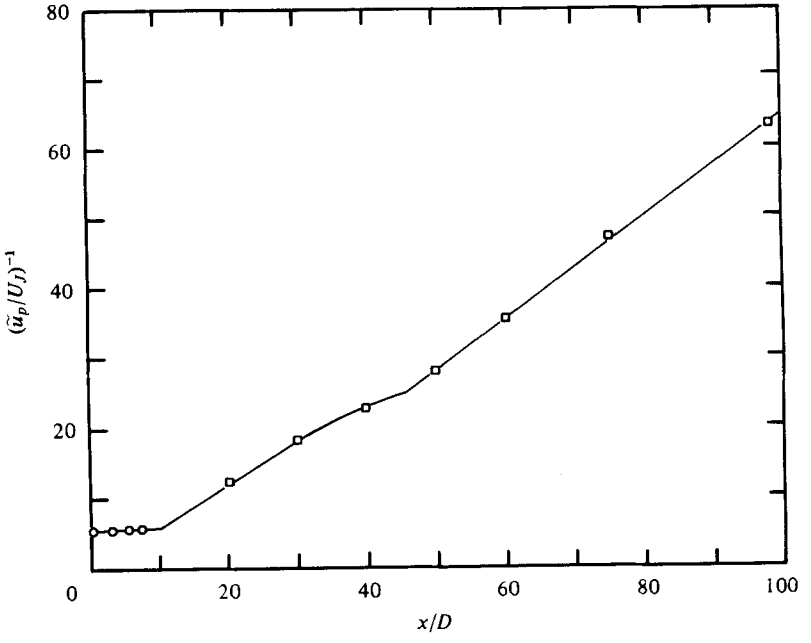

FIGURE 21. $(\tilde{u}_p/U_J)^{-1}$ *vs.* x/D. ($M_J = 0{\cdot}15$ to $0{\cdot}5$.) ○, present results; □, Wygnanski & Fiedler.

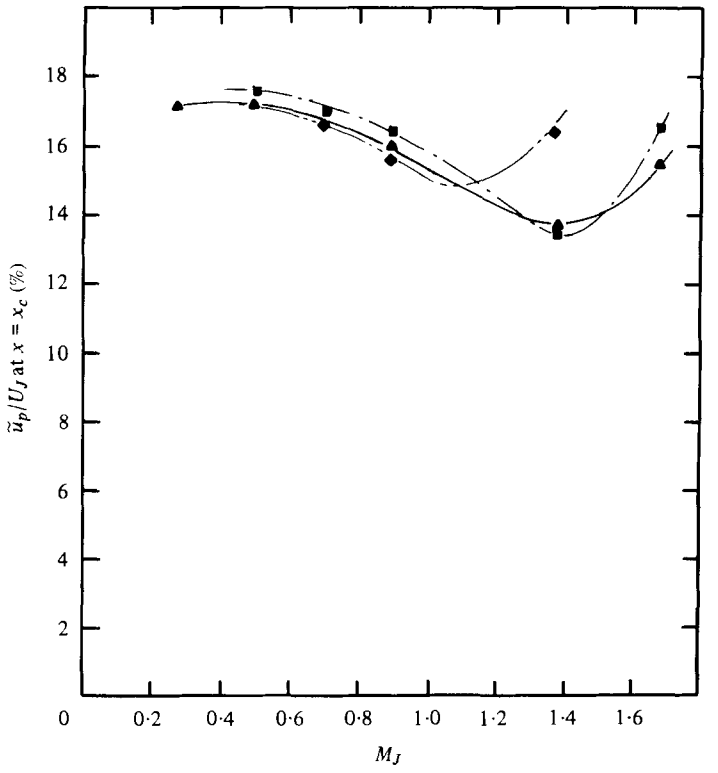

FIGURE 22. Variation of the peak axial turbulence intensity at $x = x_c$ with Mach number. T_J/T_0: ▲, 1·0; ■, 1·5; ◆, 2·32.

and the other lies in the middle and outer portions of the mixing region. The inner branch, which is more dominant, tends to jostle the outer branch and the effect is a modulation of the velocity signature in the region where the outer component is located. Thus, the turbulence intensity in the mixing region is affected by this interaction until the inner component dissipates itself at about two potential-core lengths and a new situation develops downstream.

Based on the data in figure 20 for jets at Mach 0·3 to 1·4 two expressions may be derived to describe the change of $\tilde{u}_p/U_J$ with x and M_J:

for $1{\cdot}5 < x \leqslant 2{\cdot}4x_c$,

$$\tilde{u}_p/U_J = 0{\cdot}164M_J^{-0{\cdot}1028}\exp[-0{\cdot}0016(x/D)^2]; \tag{3}$$

for $x \geqslant 2{\cdot}4x_c$

$$\tilde{u}_p/U_J = 0{\cdot}394M_J^{-0{\cdot}1028}\frac{x_c}{x}\exp[-0{\cdot}00922(x_c/D)^2]. \tag{4}$$

(In view of the change in slope in Wygnanski & Fiedler's data at $x/D \approx 35$, equation (4) is expected to be valid only up to $x = 8x_c$.)

The peak turbulence intensity of heated jets also falls with increasing axial distance, but the rate of fall does not seem to follow a consistent pattern. It is not possible

therefore to document temperature effects in the form of empirical expressions at this juncture.

One of the problems of trying to understand the significance of Mach-number or temperature effects is that the flow field also stretches or contracts depending on how the exit Mach number and temperature are changed. For instance, increasing the Mach number or decreasing the temperature ratio causes the flow field to stretch. Therefore changes in the turbulence intensity observed at a fixed point in space contain not only the substantive changes to the fluctuating flow field but also those changes which are caused by the stretching or contraction of the field.

In an effort to try to observe the substantive changes in turbulence apart from these extraneous effects, the peak turbulence intensities at the end of the potential core ($x = x_c$) are plotted in terms of M_J and T_J/T_0 in figure 22. The peak turbulence initially falls with increasing Mach number and there is little distinction between the curves for different jet temperature ratios. But, as the Mach number is increased further, each curve begins to peel off. The peak turbulence reaches a trough in each case and subsequently rises. At the locations of the respective troughs, the convection velocity of the structure in the jet is in the order of the ambient speed of sound. It appears possible therefore that the subsequent rise in the peak turbulence intensity may be associated with the 'eddies' convecting supersonically. It may be recalled that the spreading rate (δ_η) also shows an upturn at this condition. This suggests an affinity between δ_η and $\tilde{u}_p$ but it would also imply that turbulence falls with increasing maximum mean shear, $(\partial U/\partial r)_{\max}$, which is rather unexpected.

5.2. *Axial distributions*

Axial distributions of the turbulence intensity follow predictable trends. The intensity rises with x, reaches a peak at about $x = 2x_c$ and falls. For a given Mach number, the distribution contracts towards the nozzle exit plane as the jet temperature ratio is increased. The amount of shift in the position of the peak, for the different temperature ratio changes, conforms with observed changes in x_c. The magnitude of the peaks rises in general with the exit temperature ratio.

The various distributions for jets of different exit conditions may also be reduced to a band (with the same degree of scatter as shown in figure 19) when plotted in terms of $\tilde{u}_a/\tilde{u}_{ap}$ or $\tilde{v}_a/\tilde{v}_{ap}$ and x/x_c, $\tilde{u}_{ap}$ and $\tilde{v}_{ap}$ being the peak value in each distribution.

The variation of $\tilde{u}_{ap}$ and $\tilde{v}_{ap}$ with M_J and T_J/T_0 is shown in figure 23. In each case, at low Mach numbers, the peak value falls with increasing Mach number, the fall being steeper as the exit temperature ratio is increased. At high Mach numbers, the peaks seem to attain an asymptotic value.

6. Conclusion

The present work is part of a continuing effort which has arisen out of a desire to know more about how the distributions of jet characteristics change as a result of a changing jet condition and to establish empirical relationships where possible to describe these changes. The experiments were conducted over a wide range of jet-exit conditions (figure 1), and a laser velocimeter was used: primarily because of its capability in measuring both mean and fluctuating velocities and also because a hot-

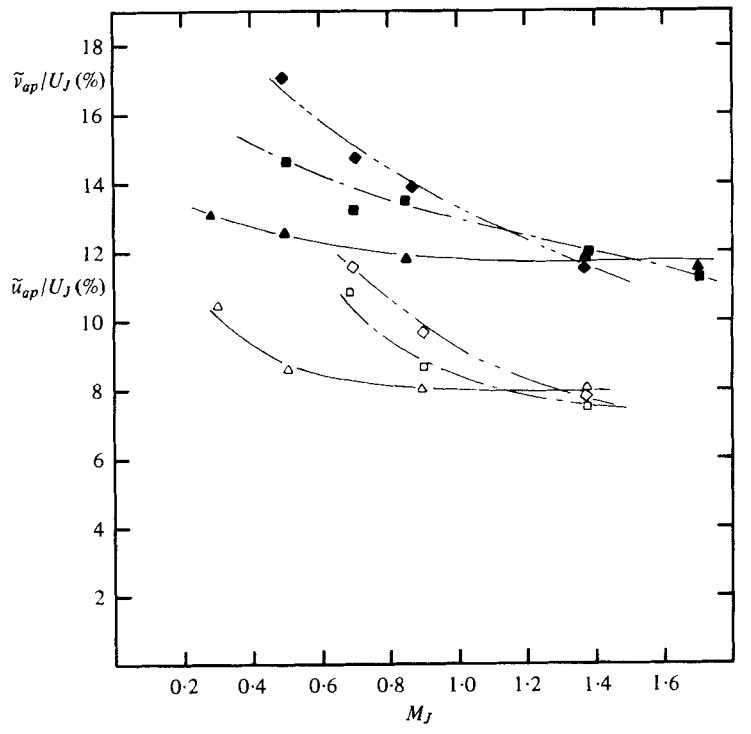

FIGURE 23. Variation of the peak turbulence intensities on the centre-line with Mach number: $\tilde{u}_{ap}/U_J$ and $\tilde{v}_{ap}/U_J$ (open symbols). T_J/T_0: ▲, 1·0; ■, 1·5; ◆, 2·32.

wire could not be used under the more severe conditions. The preliminary findings were reported in I, which was concerned with the effects of Mach number change on isothermal ($T_J/T_0 = 1$) jets. In the present paper, the effects of Mach number are considered in greater detail and, in addition, new information is made available on the effects of jet heating.

It appears that radial distributions of the mean velocity of heated jets also tend to collapse when plotted in terms of U/U_J and $\eta^* = (r - r_{0\cdot5})/x$, and this aspect of the distributions extends to about two potential-core lengths from the nozzle exit plane, as in the case of isothermal jets. Moreover, when the data from jets of varying exit conditions are plotted in terms of $\sigma\eta^*$ (σ being the Görtler spreading parameter) they fall very compactly in one universal curve.

The spreading rate (δ_η), which by definition is equal to $\sqrt{(\pi)}/\sigma$, initially falls with increasing M_J for a fixed temperature ratio (T_J/T_0) but subsequently reaches a trough and begins to rise when the jet conditions are such that the convection velocity of the large-scale structure in the jet is equal to the ambient speed of sound. The behaviour is especially noticeable in the jets at $T_J/T_0 = 1{\cdot}0$ and $1{\cdot}5$. By and large, the spreading rate falls with increasing T_J/T_0 for subsonic flows and rises for supersonic flows.

Axial distributions of the mean velocity also tend to collapse when plotted in terms of U/U_J and x/x_c (x_c being the potential length), but the data are more scattered than for the radial distributions, or for similar distributions from isothermal jets alone. The

same Kleinstein–Witze curve derived for isothermal jets (I) passes through the middle of the narrow band of data points.

The potential core contracts generally when the jet-exit temperature is increased, or the exit Mach number decreased. These variations in the potential-core length and the spreading rate of the mixing region are used to study the movement of the mixing-region boundaries as the exit conditions are changed and it appears that the shear layer undergoes not only expansion and contraction but also rotation.

Radial distributions of the turbulence also tend to collapse when plotted in terms of $\tilde{u}/\tilde{u}_p$ and $\sigma\eta^{**}$, $\tilde{u}_p$ being the peak value of the turbulence at a given station. The radial parameter η^{**} is related to the position of the peak rather than the half-velocity point because in the heated jets the peaks in many cases are located at some distance from $r_{0.5}$.

The peak turbulence falls with increasing axial distance. Initially, the fall is very gradual, but from about two potential-core lengths it varies as $1/x$. The sudden change in behaviour around this position was also noticed in the radial distributions of mean velocity (I), and lends support to a suggestion that the jet structure undergoes a radical change at about this station (Lau 1979).

The peak turbulence in the plane at the end of the potential falls initially with increasing Mach number and there is no significant difference in the results between jets of different temperatures. However, it reaches a trough in each case at a Mach number which corresponds to the large-scale eddy convection velocity being equal to the ambient speed of sound. From this and the earlier results on the spreading rate, it would seem therefore that a change in the structure of the jet may occur at this condition. The nature of the change is however unclear at present.

Centre-line distributions of the turbulence also have a tendency to collapse when plotted in terms of $\tilde{u}_a/\tilde{u}_{ap}$ and x/x_c, $\tilde{u}_{ap}$ being the peak turbulence.

The work is financed by the AFAPL under Contract F33615-76-C-2021 monitored originally by Mr Paul Shahady and recently by Lt. R. McGregor. The author wishes to thank Messrs M. C. Whiffen, D. M. Smith, and L. V. Mazzarella for their help in the course of the experimental work and Messrs R. H. Burrin and J. Mehta and Mrs B. Reagan for their part in the preparation of this paper. Thanks are also due to Dr H. E. Plumblee, the project manager, for his encouragement.

REFERENCES

Abramovich, G. N. 1963 *The Theory of Turbulent Jets.* Massachusetts Institute of Technology Press.

Barnett, D. O. & Giel, T. V. 1976 *Arnold Engng Development Center Rep.* no. AEDC-TR-76-36.

Batt, R. G. 1977 *J. Fluid Mech.* **82**, 53.

Birch, S. F. & Eggers, J. M. 1972 *N.A.S.A.* SP-321, 11.

Bradshaw, P., Ferris, D. H. & Johnson, R. E. 1964 *J. Fluid Mech.* **19**, 591.

Cary, B. B. 1954 Ph.D. thesis, University of Maryland.

Corrsin, S. & Kistler, A. L. 1955 *N.A.C.A. Rep.* 1244.

Eggers, J. M. 1966 *N.A.C.A. Tech. Note* D-3601.

Korst, H. H. & Chow, W. L. 1962 *Univ. of Illinois Mech. Eng. Rep.* TN 393–2.

Lau, J. C. 1978 *A.I.A.A. Paper* no. 78–1152.

Lau, J. C. 1979 *Proc. Roy. Soc.* A **368**, 547.

LAU, J. C. 1980 Laser velocimeter correlation measurements in subsonic and supersonic jets. *J. Sound & Vib.* **70**, 85.

LAU, J. C., MORRIS, P. J. & FISHER, M. J. 1979 *J. Fluid Mech.* **93**, 1. (See also 1976 *A.I.A.A. Paper* no. 76–348.)

LAU, J. C., WHIFFEN, M. C., FISHER, M. J. & SMITH, D. M. 1981 *J. Fluid Mech.* **102**, 353.

TANNA, H. K. 1977 *J. Sound & Vib.* **50**, 405.

WHIFFEN, M. C., LAU, J. C. & SMITH, D. M. 1979 *Laser Velocimetry and Particle Sizing, Proc. 3rd Int. Workshop on Laser Velocimetry, Purdue Univ.* 1978, p. 197. Hemisphere.

WITZE, P. O. 1974 *A.I.A.A. J.* **12**, 417.

WYGNANSKI, I. & FIEDLER, H. 1969 *J. Fluid Mech.* **38**, 577.